

## Article

# Green Production of Biodiesel from High Acid Value Oil via Glycerol Esterification and Transesterification Catalyzed by Nano Hydrated Eggshell-Derived CaO

Zhenghui Weng, Yuanzhe Tao, Haotian Fei , Weishan Deng, Yiyao Chen, Zhiqi Zhao, Xiaojiang Liang and Yong Nie \* 

Biodiesel Laboratory of China Petroleum and Chemical Industry Federation, Zhejiang Provincial Key Laboratory of Biofuel, College of Chemical Engineering, Zhejiang University of Technology, Hangzhou 310014, China; 201906022727@zjut.edu.cn (Z.W.); 201906020320@zjut.edu.cn (Y.T.); 2112001421@zjut.edu.cn (H.F.); 201906020501@zjut.edu.cn (W.D.); 201906020902@zjut.edu.cn (Y.C.); 201906020826@zjut.edu.cn (Z.Z.); lxj0824@zjut.edu.cn (X.L.)

\* Correspondence: ny\_zjut@zjut.edu.cn; Tel.: +86-13675897635

**Abstract:** Biodiesel is a widely recognized and favored liquid biofuel, primarily attributed to its biodegradability and non-toxicity. However, the development of biodiesel is hindered by its high production costs. Here, we developed a method that combines glycerol esterification and transesterification reaction catalyzed using nano-hydrated CaO for the green production of biodiesel from high acid value oil. Waste eggshell was chosen as the calcium source to examine the effect of hydration temperature and duration. The catalysts were optimized using a synthesis process involving under calcination for 3 h at 875 °C, followed by hydration at 60 °C for 6 h and subsequent dehydration at 725 °C. The catalyst loading, alcohol-to-oil mass ratio, reaction temperature, and duration were optimized to 2.5 wt%, 35%, 60 °C, and 2 h, respectively. Under the optimized conditions, the yield of fatty acid methyl ester reached 94.44%. The catalyst was successfully reused eight cycles while maintaining a yield of fatty acid methyl ester at 80.52%. In addition, a comprehensive overview was summarized to compare the catalyst preparation methods, reaction conditions, biodiesel yield, and reusability in the production of biodiesel using eggshell-derived CaO.

**Keywords:** biodiesel; high acid value oil; biobased calcium oxide; transesterification; hydration



**Citation:** Weng, Z.; Tao, Y.; Fei, H.; Deng, W.; Chen, Y.; Zhao, Z.; Liang, X.; Nie, Y. Green Production of Biodiesel from High Acid Value Oil via Glycerol Esterification and Transesterification Catalyzed by Nano Hydrated Eggshell-Derived CaO. *Energies* **2023**, *16*, 6717. <https://doi.org/10.3390/en16186717>

Academic Editor: João Fernando Pereira Gomes

Received: 21 August 2023

Revised: 12 September 2023

Accepted: 14 September 2023

Published: 20 September 2023



**Copyright:** © 2023 by the authors. Licensee MDPI, Basel, Switzerland. This article is an open access article distributed under the terms and conditions of the Creative Commons Attribution (CC BY) license (<https://creativecommons.org/licenses/by/4.0/>).

## 1. Introduction

Due to the limited availability of conventional fossil fuels and increasing concerns regarding ecological conservation, many countries are transitioning from fossil fuels to renewable energy sources [1]. Meeting the current energy demand has led to an increased focus on developing and utilizing green and clean energy sources, such as solar energy and wind power. However, the challenge of weather and seasonal changes causing an unstable supply of these energy sources remains a significant concern. Consequently, utilizing clean and environmentally sustainable biomass fuels as a viable alternative to fossil fuels is considered an advantageous approach for reducing carbon emissions [2,3]. Fatty acid methyl ester (FAME) has gained considerable interest as the most prevalent biobased eco-friendly fuel, primarily attributed to its excellent lubricity, non-toxicity, and biodegradability, usually produced by the transesterification reaction between triglycerides and methanol using a base catalyst (Figure 1) [4,5].

It has been reported that the production cost of biodiesel is higher than that of petrochemical diesel, which hampers its large-scale development [6]. Feedstock expenses constitute approximately 80% of the total cost, underscoring the potential of utilizing waste oils and fats to effectively reduce production costs [1,7]. However, the high free fatty acids (FFAs) content in waste oils and fats poses a significant challenge due to the potential

for saponification reactions during transesterification reactions, leading to a decreased yield of FAME. Consequently, the necessity for pretreatment methods to mitigate the acid value of waste oils is evident [6]. To overcome these issues, a two-step biodiesel production method has been developed [8,9]. In the first step, FFAs are esterified with glycerol, forming monoglycerides, diglycerides, and triglycerides (Figure 2). Subsequently, the glycerides are transesterified with methanol to form FAME. Glycerol esterification serves as a practical pretreatment approach, capitalizing on the by-product of transesterification to reduce acid value. This method eliminates the need for concentrated sulfuric acid, acid, and excessive methanol while also requiring less specialized equipment compared to the conventional direct esterification of FFAs and methanol [10].

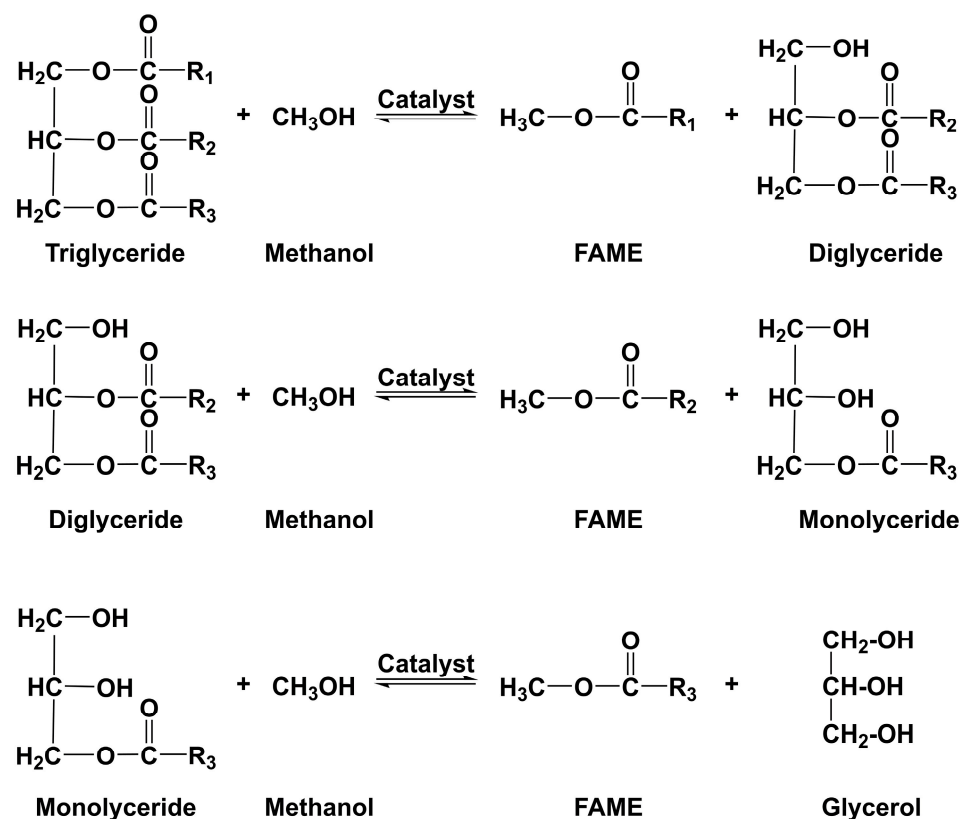


Figure 1. The basic transesterification reaction.

Homogeneous base catalysts such as NaOH and KOH have gained widespread usage in the biodiesel industry due to their high catalytic activity [11,12]. However, these catalysts face challenges such as catalyst loss, limited reusability, reactor corrosion, and environmental pollution, which hinder further cost reduction and efficiency improvement [13–15]. Consequently, the development of cost-effective, reusable, and environmentally friendly heterogeneous catalysts has emerged as a prominent research area in recent years [3,16–19]. Calcium oxide is extensively researched as a green heterogeneous base catalyst for transesterification reactions due to its environmentally friendly nature, non-toxicity, affordability, and effective catalytic activity [20–23]. CaO is abundant in the form of limestone found in rock formations [20,21,24]. Additionally, CaO can be derived from biological sources such as bone, exoskeletons, and eggshells, which have been reported to be more environmentally friendly [25–29]. Among these sources, catalysts prepared from waste eggshells exhibit higher surface calcium yields compared to those from waste crab shells, making eggshell-derived CaO more efficient in catalysis [30]. However, while CaO catalysts prepared using direct calcination from biological resources can achieve a high yield of FAME, they require higher catalyst loading and longer duration. This is primarily attributed to the catalyst's relatively low specific surface area and basic strength [31].

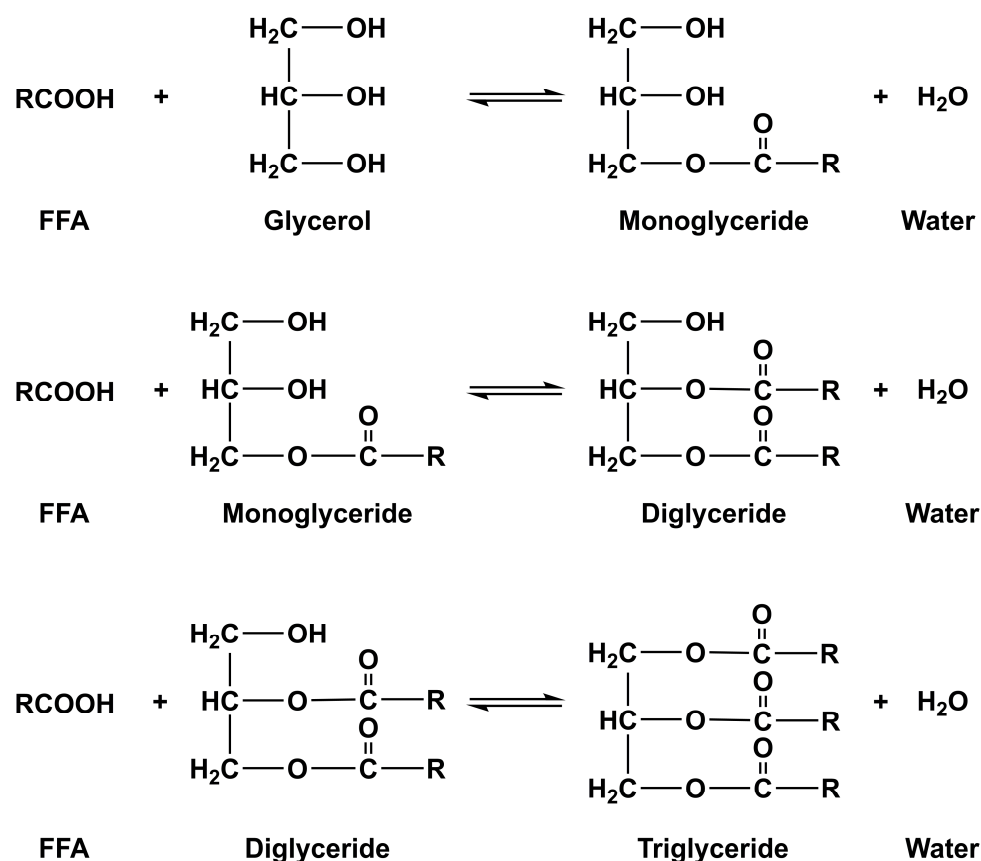


Figure 2. The basic glycerol esterification.

Hydration-dehydration technique has been reported as an effective method to enhance the catalytic activity of CaO catalysts derived from biowaste, resulting in improved basic strength and specific surface area for transesterification reaction [32,33]. The hydration-dehydration process has been found to significantly reduce catalyst crystallinity and increase specific surface area, as demonstrated by Ashine et al. [34]. Despite the evident advantages of this technique, its full potential remains largely unexplored in the literature. While previous studies have demonstrated its convenience and cost-effectiveness in achieving higher catalytic activity and milder reaction conditions [31–35], there is a noticeable gap in the existing research concerning the optimization of hydration-dehydration conditions for these catalysts. This gap presents an opportunity for further investigation and refinement, aiming to unlock the full catalytic potential of CaO catalysts derived from biowaste.

In this work, an approach that combined glycerol esterification and transesterification reaction for biodiesel production from high acid value oil was developed. Waste eggshells were utilized as the raw material to prepare a series of hydrated CaO catalysts using calcination, hydration, and subsequent dehydration processes. The structural properties of the catalysts were determined using various characterizations. The catalyst preparation conditions were optimized based on their catalytic performance and crystallite size. Further, the optimized catalyst was employed in the transesterification reaction of glycerol-esterified oil, and the reaction conditions were optimized. In addition, the reusability of the catalyst was investigated to determine its stability.

## 2. Experimental

### 2.1. Materials

The waste eggshells were obtained from the Dexin canteen located at the Moganshan campus of Zhejiang University of Technology. The model compound (with an acid value of 119.13 mg KOH/g) was mixed with soybean oil (Goldfish, China) and oleic acid (pur-

chased from Shandong Dingyu Bio-Energy Co., Ltd. (Jinan, China), with an acid value of 200 mg KOH/g) in a mass ratio of 2:3. Glycerol of pure analytical grade, methanol of pure analytical grade, and Hammett indicators were sourced from Shanghai Titan Technology Co., Ltd. (Shanghai, China).

## 2.2. Catalyst Preparation and Optimization

The waste eggshells were washed with water, followed by drying in an oven. Subsequently, the dried eggshells were ground and sieved through a 200-mesh sieve. The resulting powder was then calcined in air at 875 °C for 3 h, using a heating rate of 10 °C/min. The calcined samples were subjected to hydration under various conditions. After the hydration process, the hydrated samples were dried at 105 °C for 6 h. Finally, the hydrated samples underwent another round of calcination at 725 °C for 3 h, with a heating rate of 5 °C/min. This step aimed to produce CaO with hydration–dehydration characteristics (CaO<sub>H</sub>). To determine the optimal hydration temperature and duration, specific hydration conditions were employed. The hydrated samples were exposed to different specified temperatures (45 °C, 55 °C, 60 °C, 65 °C, 70 °C) for 6 h. This allowed for the identification of the most favorable hydration temperature within the specified hydration durations (2 h, 4 h, 6 h, 8 h).

## 2.3. Catalyst Characterization

Thermogravimetric analysis (TGA) was conducted using a Discovery TGA thermogravimetric analyzer from TA Instruments (New Castle, Delaware). The analysis was performed under an air atmosphere, employing a heating rate of 10 °C/min, within a temperature range of 32–1000 °C.

X-ray diffraction (XRD) was conducted using a Bruker AXS D8 Advance X-ray photoelectron diffractometer from Germany. The XRD measurements were performed with a tube voltage of 40 kV, scanning the range of 10–80° at a rate of 10°/min. The estimation of crystallite sizes for both the common and hydrated-dehydrated catalysts was carried out using the Debye-Scherrer equation.

N<sub>2</sub> physisorption analysis was conducted using a Mike ASAP2460 Instrument (Norcross, GA, USA). The samples underwent vacuum degassing at 200 °C for 6 h. The mean pore volume and pore size were determined using the Barrett-Joyner-Halenda (BJH) method, and the specific surface area of the samples was determined using the BET method.

The basic strength of the catalyst was assessed using the Hammett indicator method. To perform this analysis, 0.05 g of the catalyst was dissolved in 0.5 mL of a solution containing Hammett indicator, which was further diluted in 10 mL of methanol. The solution was allowed to stand for a sufficient period of time to ensure system equilibration. Once the system's color reached a stable state and exhibited no further changes, it was compared to the acid-base color of the indicator to determine the catalyst's basic strength.

Scanning electron microscopy (SEM) analysis was performed using a Czech TESCAN (Brno, Czech Republic) desktop scanning electron microscope for specimen characterization.

## 2.4. Glycerol Esterification of Feedstock

To reduce the acid value, glycerol esterification was employed to obtain glycerol-esterified oil. The feedstock was mixed with glycerol in a mass ratio of 4:1, and the resulting mixture was preheated to 240 °C under a nitrogen flow rate of 200 mL/min. Rotation speed was set at a rate of 500 r/min, and the reaction was initiated at 240 °C. The reaction was maintained under these conditions for 3 h to ensure that the acid value of the product was below 1 mg KOH/g. To obtain glycerol-esterified oil, the glycerol was subsequently distilled under high vacuum conditions (20–80 Pa). The acid value of the samples was determined using titration following the national standard GB/T 5530 [36].

The composition analysis of the glycerol-esterified oil was determined using a Shimadzu LC-20AT high-performance liquid chromatography (HPLC) system. A Kromasil NH<sub>2</sub> column (250 mm × 4.6 mm, 5 μm) and a refractive index detector (RID) were em-

ployed. The mobile phase consisted of hexane and isopropanol (9:1, *v:v*), flowing at a rate of 0.8 mL/min. A sample injection volume of 10  $\mu$ L was used, and the oven temperature was maintained at 35 °C. The composition of monoglycerides, diglycerides, and triglycerides was determined using the area normalization method.

### 2.5. Catalytic Tests and Product Analysis

The transesterification reaction of the glycerol-esterified oil was conducted using a 50 mL three-neck flask equipped with a reflux condenser, magnetic stirrer, and thermometer. Methanol and the catalyst were mixed at 500 r/min and preheated to a specified temperature (50–65 °C). Subsequently, 20 mL of glycerol-esterified oil was added to the three-neck flask, and the moment when all the oil had been added was considered the starting point of the reaction. The effect of different variables was explored for the transesterification reaction, including catalyst loading (1.5–3.5 wt%), alcohol-to-oil mass ratio (25–45%), reaction temperature (50–65 °C), and corresponding reaction duration (1–3 h) in several separate sets of experiments. At the end of each experimental group, 1–2 mL of the reaction mixture were sampled and centrifuged to separate the catalyst from the mixture for analysis. Before analyzing the biodiesel product, any excess methanol in the mixture was spin-distilled in a water bath at 70 °C for 20 min. The FAME composition and content were determined using gas chromatography (Shimazu GC2014, Kyoto, Japan) with a flame ionization detector (FID) and a polar DB-5 capillary column (30 m  $\times$  0.25 mm, 0.25  $\mu$ m). The FAME content of the production was calculated using Equation (1) and served as the evaluation index for the FAME yield of the transesterification reaction.

$$\text{Yield of FAME (\%)} = \frac{\text{Actual FAME mass}}{\text{Theoretical FAME mass}} \gg \frac{\text{FAME concentration}}{\text{Total concentration}} \times 100\% \quad (1)$$

### 2.6. Catalyst Reusability

The reusability of the catalyst was evaluated under optimized reaction conditions. Following the completion of the reaction, the catalyst was separated from the reaction mixture using centrifugation. To remove any adsorbents, such as glycerol, glycerides, and biodiesel, the catalyst was washed with a mixed solution of methanol and hexane (in a mass ratio of 1:1). Subsequently, the catalyst was dried at 105 °C without undergoing any additional treatment.

## 3. Results and Discussion

### 3.1. Results of Glycerol Esterification

After the glycerol esterification and distillation of excess glycerol, the composition and properties of the resulting glycerol-esterified oil were analyzed and are summarized in Table 1. Using the pretreatment process, the acid value of the initial feedstock was significantly reduced from 119.13 to 0.83 mg KOH/g. This pretreatment effectively prevented catalyst deactivation and demonstrated minimal impact on the subsequent transesterification reaction [6,37]. The glycerol-esterified oil primarily comprised triglycerides, accounting for 93.44% of the total composition.

**Table 1.** Composition and properties of glycerol-esterified oil.

Index	Unit	Value
Acid value	mg KOH/g	0.83
Saponification value	mg KOH/g	199.05
Monoglyceride content	% (m/m)	2.95
Diglyceride content	% (m/m)	3.61
Triglyceride content	% (m/m)	93.44

### 3.2. Catalyst Optimization

#### 3.2.1. Catalyst Dehydration Temperature Optimization

The determination of the optimal dehydration temperature was accomplished using thermogravimetric analysis (TGA) conducted on the hydrated catalyst (Figure 3). The TGA profile exhibited two distinct mass loss regions: one spanning from 400 to 475 °C, attributed to the decomposition of  $\text{Ca}(\text{OH})_2$  into  $\text{CaO}$ , and the other ranging from 630 to 705 °C, attributed to the removal of water trapped within the crystallite structure. The cumulative mass loss observed was 25.4%, aligning well with the theoretical mass loss anticipated from the dehydration of  $\text{Ca}(\text{OH})_2$  to  $\text{CaO}$ . Notably, an increase in temperature beyond the optimal point results in catalyst sintering, which compromises its catalytic activity [38]. Consequently, based on the TGA findings, a dehydration temperature of 725 °C was selected as the optimum for the precursor, ensuring complete fragmentation of the  $\text{CaO}$  particles and maximizing catalytic efficiency.

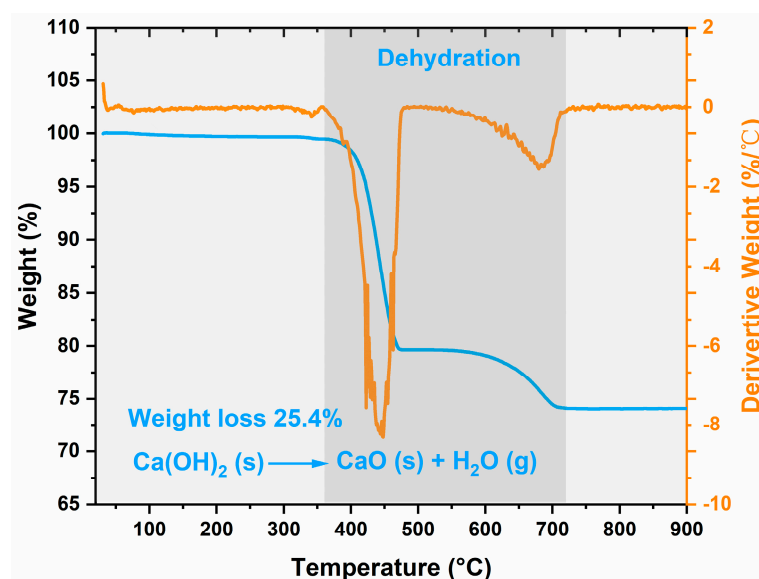
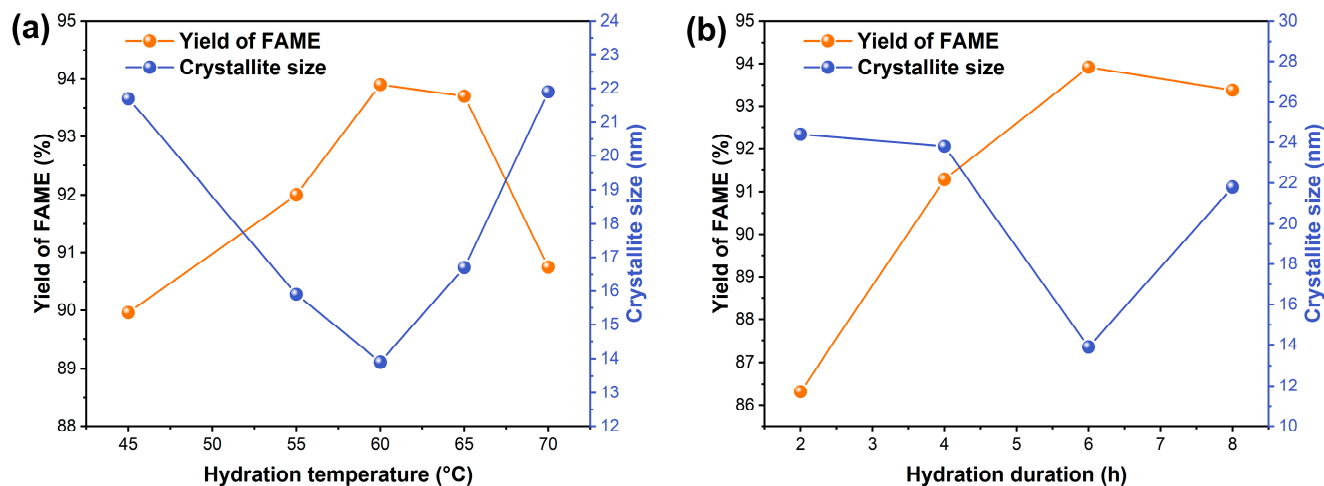


**Figure 3.** Thermogravimetric analysis of the hydrated catalyst.

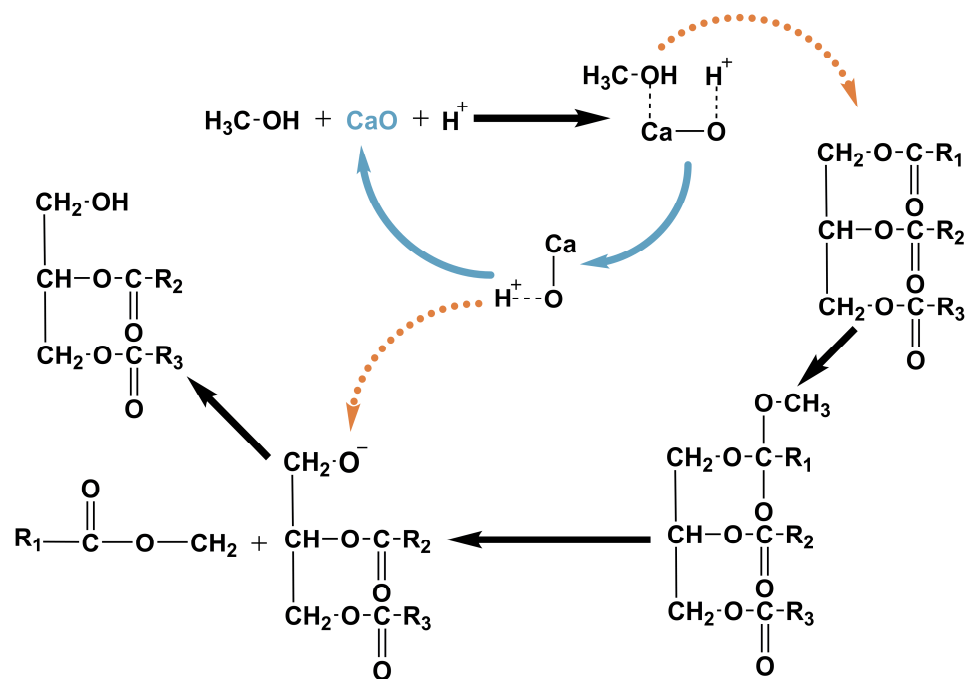
#### 3.2.2. Hydration Optimization

Figure 4a illustrates the influence of hydration temperature on the yield of FAME and crystallite size. A hydration period of 6 h was employed, and temperatures ranging from 45 °C to 70 °C were investigated. The transesterification reaction was conducted under the following conditions: rotation speed of 500 r/min, alcohol-to-oil mass ratio of 40%, reaction temperature of 60 °C, and catalyst loading of 2.5 wt%. The reaction was sustained for 2 h. The yield of FAME exhibited an upward trend as the hydration temperature increased until it reached 60 °C, where the maximum yield of 93.90% of FAME was attained. However, a decline in yield was observed as the hydration temperature was elevated beyond the optimal point. Therefore, the optimum hydration temperature was determined to be 60 °C. The catalytic mechanism is illustrated in Figure 5 [39,40]. The active site on the catalyst surface, when combined with methanol, produces a highly reactive nucleophilic methanolic anion, which is more favorable to attack the electrophilic carbonyl carbon in the triglyceride to form a diglyceride, which reacts similarly to the monoglycerides, ultimately giving the FAME [35,38,41]. Figure 4a clearly demonstrates a negative correlation between catalyst crystallite changes at different hydration temperatures and the resulting yield of FAME. The change in hydration temperature directly impacted the hydroxylation of  $\text{CaO}$ , influencing the fragmentation of the original  $\text{CaO}$  crystallites and the subsequent growth of new crystallites following further dehydration. Smaller crystallites and lower crystallinity contributed to a great number of active sites on the catalyst surface, as well as increased alkalinity, which promoted the formation of methanol anions, enhancing

overall reactivity and promoting a higher yield of FAME [22,27,42]. The crystallite size data from the XRD results corroborated this deduction. In addition, the application of lower hydration temperature facilitates the transesterification reaction while reducing the required energy input.



**Figure 4.** Optimization of hydration process: (a) hydration temperature; (b) hydration duration (Reaction conditions: rotation speed of 500 r/min, catalyst loading of 2.5 wt%, alcohol-to-oil mass ratio of 40%, reaction temperature of 60 °C and reaction duration of 2 h).



**Figure 5.** Catalytic mechanism.

During the hydration process, the duration of hydration plays a crucial role in the destruction and regeneration of catalyst crystallite [31]. Figure 4b illustrates the effect of hydration duration on the yield of FAME and crystallite size. Specifically, when the hydration temperature was set at 60 °C, hydration duration ranging from 2 h to 8 h was investigated. The transesterification reaction was carried out under conditions of a rotation speed of 500 r/min, a mass ratio of alcohol-to-oil of 40%, a reaction temperature of 60 °C, and a catalyst loading of 2.5 wt%, with a reaction duration of 2 h. As depicted in Figure 4b, with increasing hydration duration, the original crystallites were continuously destroyed, and new crystallites formed and grew. The crystallite size decreased to a minimum of

13.9 nm when the hydration duration reached 6 h, resulting in a corresponding increase in the yield of FAME to 93.92%. However, as the hydration duration was further prolonged, the destruction of original crystallites continued, accompanied by the growth of new crystallites. This led to a decrease in the density of active sites on the catalyst surface, ultimately resulting in a decline in the yield of FAME. Based on these observations, it can be concluded that the optimum hydration duration for achieving the highest yield of FAME was 6 h.

### 3.3. Catalyst Characterization

#### 3.3.1. XRD Analysis

The XRD patterns of the catalysts, including common CaO, CaO<sub>H-45-6h</sub>, CaO<sub>H-55-6h</sub>, CaO<sub>H-60-6h</sub>, CaO<sub>H-65-6h</sub>, CaO<sub>H-70-6h</sub>, CaO<sub>H-60-2h</sub>, CaO<sub>H-60-4h</sub>, CaO<sub>H-60-6h</sub>, and CaO<sub>H-60-8h</sub>, are presented in Figure 6. The results demonstrated that the catalysts prepared at different hydration temperatures and duration exhibited identical peak positions and lattice parameters to those prepared without hydration. This indicated that catalytically active species remained unaffected by the hydration temperature and duration. The crystallite sizes of both the common catalyst and each hydrated catalyst were estimated using the Debye–Scherer equation (Figure 4). The results revealed a significant reduction in the crystallite size of the hydrated-treated CaO, indicating a strong influence of hydration temperature on the crystallinity and crystallite size of the catalysts [27,32]. Furthermore, when the hydration duration was set to 6 h under different temperature conditions, no characteristic peaks of Ca(OH)<sub>2</sub> were detected. The changes in the diffraction peaks of Ca(OH)<sub>2</sub> can be found when the hydration duration varies, demonstrating the occurrence of changes in the growth and fragmentation of old and new crystallites.

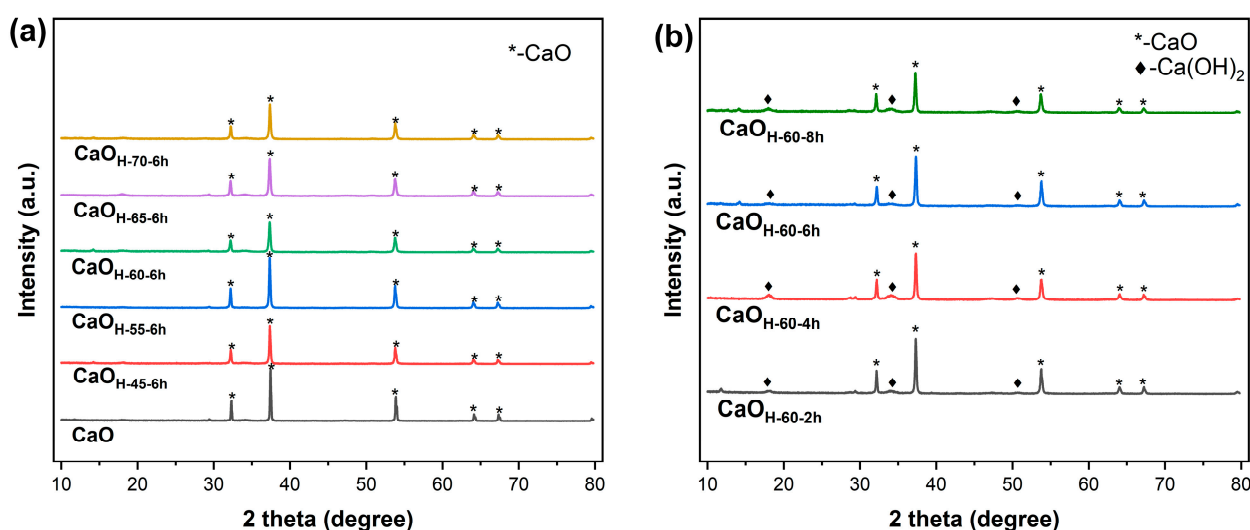


**Figure 6.** XRD patterns of the catalysts at different hydration (a) temperature and (b) duration.

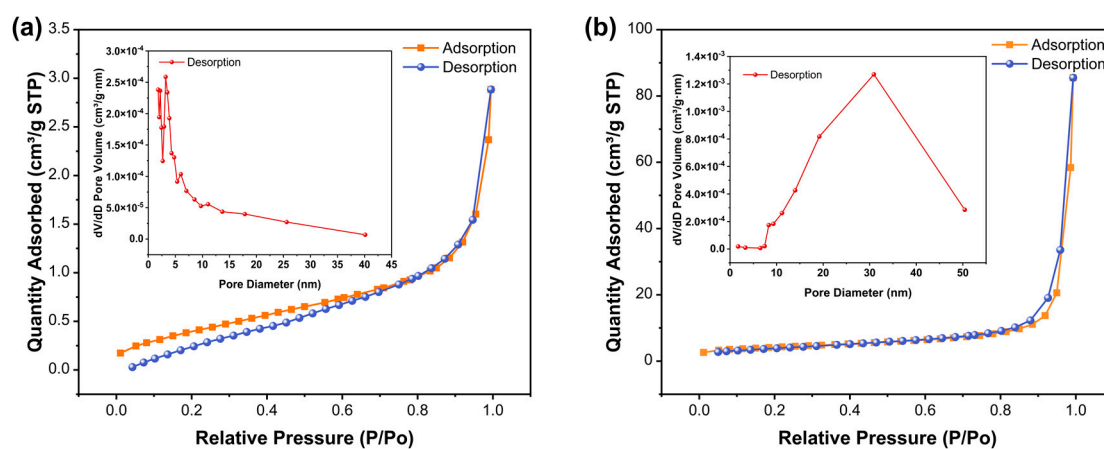
#### 3.3.2. N<sub>2</sub> Physisorption Analysis and Basic Strength Analysis

Table 2 presents the N<sub>2</sub> physisorption and basic strength analysis results, indicating that the hydration treatment rendered the CaO catalyst mesoporous, thereby facilitating the diffusion of reactants. The common catalyst exhibited a BET surface area of 1.6429 m<sup>2</sup>/g, whereas the catalyst subjected to further hydration-dehydration displayed significantly larger BET surface areas. This observation aligns with the understanding that a higher surface area exposes more active sites, leading to improved catalytic performance and higher conversion efficiency [31–33]. Thus, it can be concluded that the hydration–dehydration process enhanced the BET surface area of CaO. Furthermore, Table 2 reveals that the hydration temperature and duration also had an impact on the BET surface area, pore volume, pore size, and basic strength. The duration of hydration did not have a significant influence on the change in BET surface area or the basic strength of the catalyst. Upon optimizing

the catalyst preparation, the most favorable catalytic performance was observed with  $\text{CaO}_{\text{H-60-6h}}$ , exhibiting a basic strength within the range of 12.2–15.6 and the highest BET surface area [43,44]. However, contrary to expectations, further increasing the hydration temperature led to unexpected results despite the relatively large BET surface area of the  $\text{CaO}_{\text{H-70-6h}}$  catalyst (Figure 4a).  $\text{N}_2$  adsorption–desorption isotherms displayed a type IV isotherm shape for both common CaO and  $\text{CaO}_{\text{H-60-6h}}$ , as illustrated in Figure 7. Analysis of the BJH pore size distribution confirmed that  $\text{CaO}_{\text{H-60-6h}}$  exhibits larger mesoporous structures in comparison to common CaO.

**Table 2.**  $\text{N}_2$  physisorption and basic strength analysis of catalysts.

Catalyst	BET Surface Area ( $\text{m}^2/\text{g}$ )	Mean Pore Diameter (nm)	Total Pore Volume ( $\text{cm}^3/\text{g}$ )	Basic Strength
CaO	1.6429	10.8644	0.004449	$9.3 < \text{H}_- < 12.2$
$\text{CaO}_{\text{H-45-6h}}$	11.6408	48.2618	0.135590	$9.3 < \text{H}_- < 12.2$
$\text{CaO}_{\text{H-55-6h}}$	9.6729	50.4828	0.077243	$12.2 < \text{H}_- < 15.6$
$\text{CaO}_{\text{H-60-6h}}$	14.8209	43.8119	0.130846	$12.2 < \text{H}_- < 15.6$
$\text{CaO}_{\text{H-65-6h}}$	12.4565	40.6488	0.111106	$12.2 < \text{H}_- < 15.6$
$\text{CaO}_{\text{H-70-6h}}$	13.9873	29.0470	0.106863	$9.3 < \text{H}_- < 12.2$
$\text{CaO}_{\text{H-60-2h}}$	13.7889	45.9859	0.110861	$12.2 < \text{H}_- < 15.6$
$\text{CaO}_{\text{H-60-4h}}$	12.4309	36.4223	0.084373	$12.2 < \text{H}_- < 15.6$
$\text{CaO}_{\text{H-60-8h}}$	12.8146	41.8096	0.093936	$12.2 < \text{H}_- < 15.6$



**Figure 7.**  $\text{N}_2$  adsorption–desorption isotherm and pore diameter distribution of (a) CaO and (b)  $\text{CaO}_{\text{H-60-6h}}$ .

### 3.3.3. SEM Analysis

The SEM images presented in Figure 8 depict the morphologies of the common CaO catalyst, as well as the  $\text{CaO}_{\text{H-60-6h}}$ ,  $\text{CaO}_{\text{H-45-6h}}$ , and  $\text{CaO}_{\text{H-70-6h}}$  catalysts after calcination at  $725^\circ\text{C}$ . The common catalyst (CaO) exhibited a spindle-like agglomerate structure with large particles, limited pore structure, and a larger particle diameter, averaging between 0.5–1  $\mu\text{m}$ . This morphology aligned with the low specific surface area determined using  $\text{N}_2$  physisorption analysis. Conversely, the hydrated catalysts displayed distinct grain morphologies characterized by smaller particle sizes and a honeycomb-like porous structure, which corresponded to the high specific surface area determined using  $\text{N}_2$  physisorption analysis. The formation of this porous structure can be attributed to the decomposition of  $\text{Ca}(\text{OH})_2$  and the release of bound water from the calcium oxide at elevated temperatures. The activity of gaseous water molecules during this process disrupted the original cluster structure, resulting in increased porosity that enhances the catalytical effect of the

reaction [31,32]. Particle size analysis revealed that the hydration temperature influenced the particle sizes. Although the average particle sizes of the catalysts prepared at hydration temperatures of 45, 60, and 70 °C were within the range of 80–100 nm, the catalyst prepared at a hydration temperature of 60 °C exhibited a smaller average particle size of 82.66 nm, which was consistent with the smaller crystallite size observed in the XRD results.

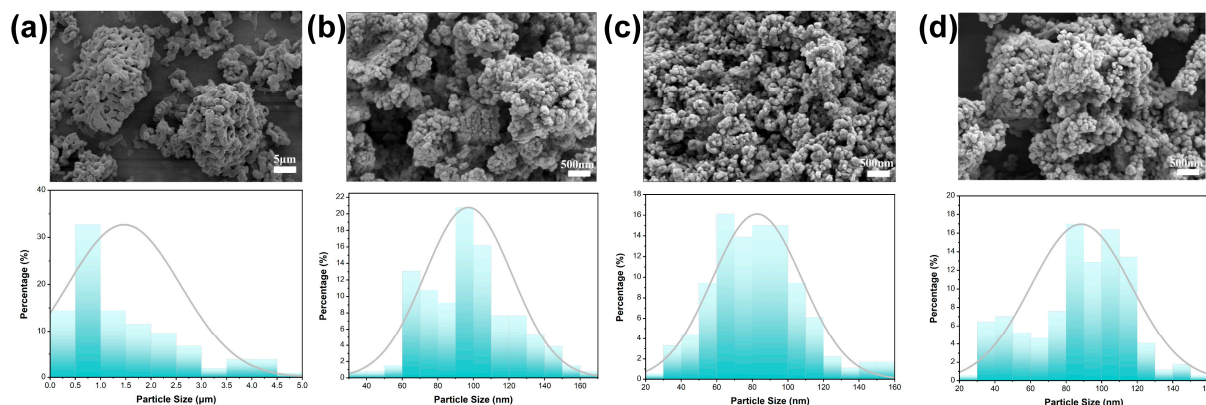


**Figure 8.** SEM images of (a) CaO; (b) CaO<sub>H-45-6h</sub>; (c) CaO<sub>H-60-6h</sub>; and (d) CaO<sub>H-70-6h</sub> (details of CaO and CaO<sub>H-60-6h</sub> see Figures S1 and S2).

### 3.4. Transesterification Process Optimization

#### 3.4.1. Catalyst Loading

Under the reaction conditions of a rotation speed of 500 r/min, a mass ratio of alcohol-to-oil of 40%, a reaction temperature of 60 °C, and a duration of 2 h, the effect of catalyst loading on the yield of FAME was investigated. As depicted in Figure 9a, increasing the catalyst loading from 1.5 wt% to 2.5 wt% resulted in an enhancement of the yield of FAME. The yield of FAME reached 91.85% when the catalyst loading was 1.5 wt%. The maximum yield of FAME of 94.07% was achieved when the catalyst loading was 2.5 wt%. This increase in yield can be attributed to the availability of more effective active sites for the reaction at higher catalyst loading, leading to increased efficiency. However, when the catalyst loading exceeded 2.5 wt%, the yield of the FAME trend began to decline. This can be attributed to the overall mass transfer resistance in the system, where the mass transfer limitation between the reactants and the catalyst became the rate-controlling step compared to the intrinsic reaction [35]. Therefore, the optimal catalyst loading was determined to be 2.5 wt%.

#### 3.4.2. Alcohol-to-Oil Mass Ratio

In practical biodiesel production, the mass ratio of methanol to oil plays a crucial role in determining the biodiesel yield. Although a theoretical alcohol-to-oil mass ratio can be calculated based on the stoichiometric ratio using the composition of mono-, di- and triglycerides in the oil, additional methanol is typically employed to promote the positive equilibrium towards biodiesel production. Therefore, relying solely on the molar ratio provides limited guidance in the actual process [31]. The effect of the alcohol-to-oil mass ratio on the yield of FAME was investigated, as shown in Figure 9b. Maintaining the reaction for 2 h at a rotation speed of 500 r/min, a catalyst loading of 2.5 wt%, and a reaction temperature of 60 °C, the results revealed an optimal alcohol-to-oil mass ratio of 35%. Within the range of 25–45 wt%, the yield of FAME remained consistently around 90%, with a peak value of 93.73% achieved at the 35% alcohol-to-oil mass ratio. Beyond the 35 wt% mark, it was presumed that excess methanol diluted the reaction system. This dilution restricts the interaction between glycerides and catalytically active sites, consequently hindering the reaction between methanol and the oil and reducing the overall yield [45]. Therefore, based on these findings, the optimal alcohol-to-oil mass ratio was determined to be 35%.

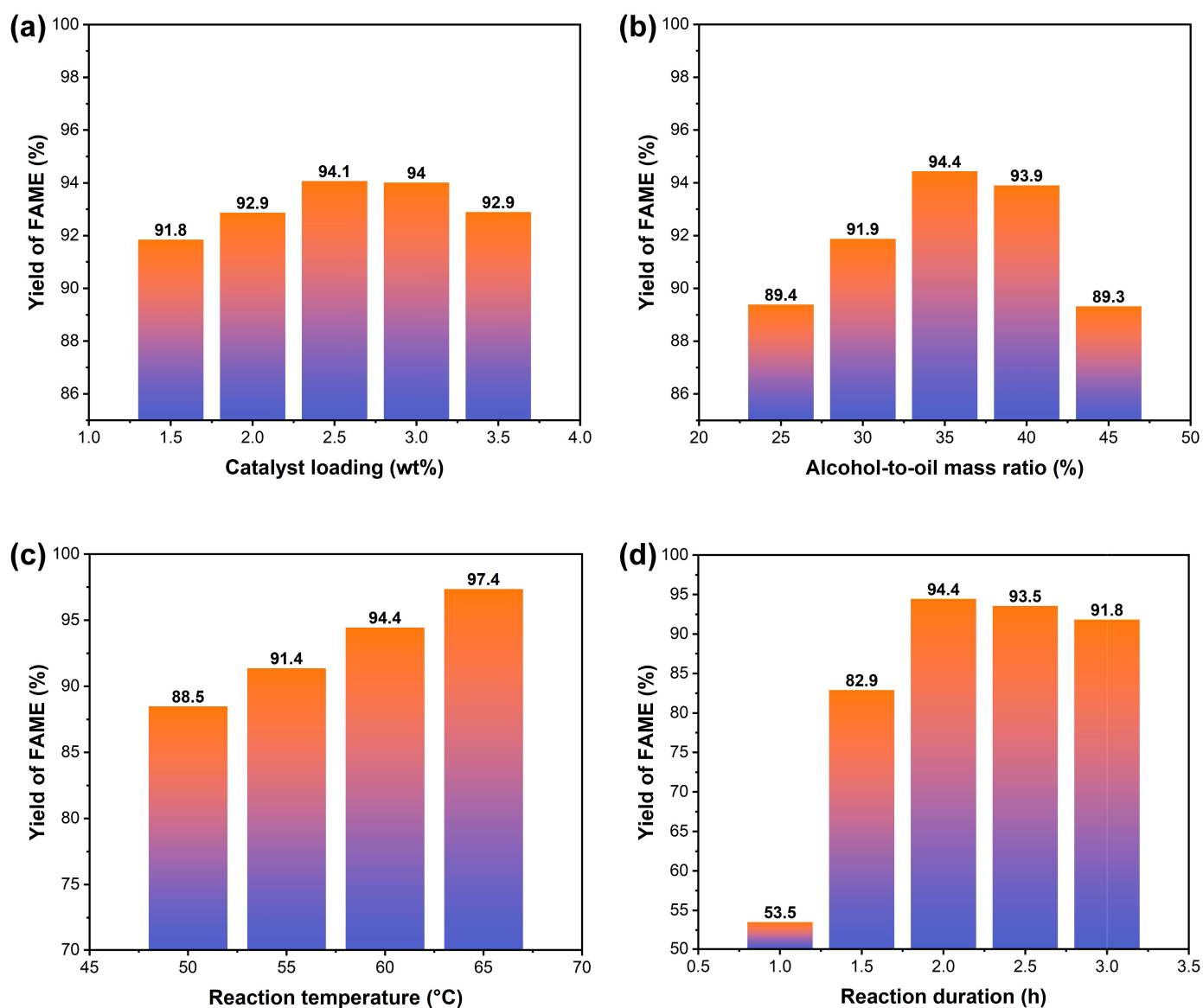


**Figure 9.** Optimization of transesterification: (a) catalyst loading; (b) alcohol-to-oil mass ratio; (c) reaction temperature; (d) reaction duration.

### 3.4.3. Reaction Temperature

The effect of the reaction temperature on the yield was investigated by maintaining the reaction for 2 h at a rotation speed of 500 r/min, an alcohol-to-oil mass ratio of 35%, and a catalyst loading of 2.5 wt%. The temperature range examined spanned from 50 °C to 65 °C, as illustrated in Figure 9c. The results demonstrated a gradual increase in yield as the reaction temperature was elevated. This observation aligned with the expected influence of reaction temperature on reaction kinetics, where higher temperature enhanced the kinetic energy of molecules in the system, facilitating more effective collisions between reactants and leading to an increased yield [35,45,46]. A remarkable yield of approximately 97.36% was attained at a reaction temperature of 65 °C. However, it is noteworthy that operating at such a high temperature surpasses the boiling point of methanol (64.7 °C at atmospheric pressure). This requires the use of additional cooling utilities and leads to increased energy consumption per unit in industrial-scale production. Consequently, the optimal reaction temperature was determined to be 60 °C.

#### 3.4.4. Reaction Duration

The effect of reaction duration on the yield of FAME was investigated while maintaining a rotational speed of 500 r/min, an alcohol-to-oil mass ratio of 35%, a catalyst loading of 2.5 wt%, and a reaction temperature of 60 °C. As depicted in Figure 9d, the highest yield of FAME of 94.44% was achieved within a reaction duration of 2 h. However, a slight decrease in the yield of FAME was observed when the reaction duration exceeded 2 h. This phenomenon may be attributed to the increasing presence of glycerol, which affects the equilibrium as the duration of the transesterification reaction extends [35]. Therefore, the optimal reaction duration was determined to be 2 h.

#### 3.5. Catalyst Reusability

The reusability of CaO as a heterogeneous catalyst in the transesterification reaction was investigated to assess its practicality and potential for large-scale biodiesel production [47]. As shown in Figure 10, the catalyst exhibited consistent performance with a yield exceeding 80% even after eight cycles of reuse. Thus, the prepared catalysts have productive reusability, indicating that the hydration–dehydration of CaO has the potential for large-scale production as a heterogeneous base catalyst for biodiesel production [33,48]. It should be noted, however, that some degree of catalyst deactivation was observed during the reusability experiments, warranting further investigation in future studies.

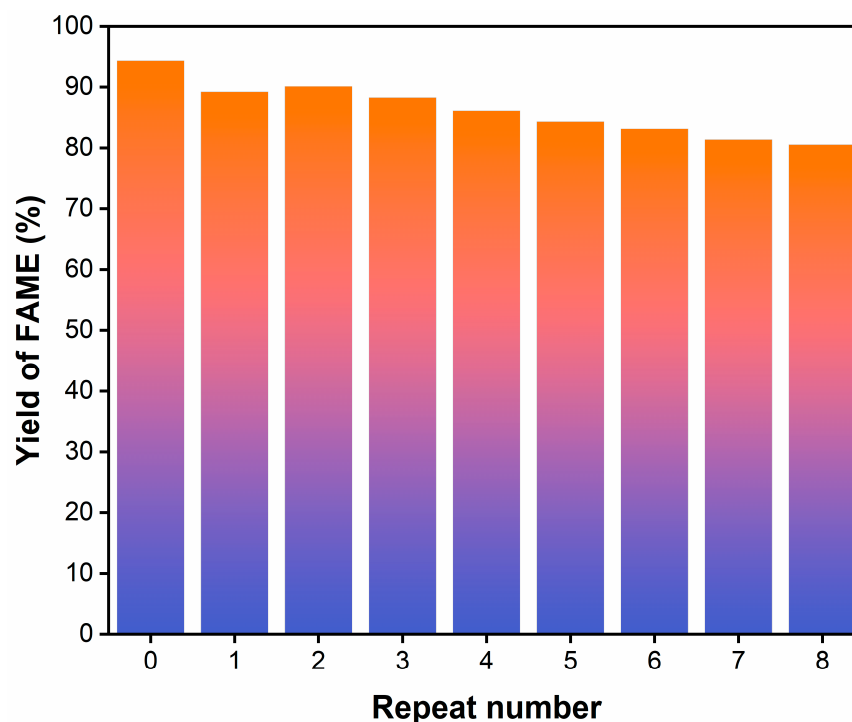


**Figure 10.** Reusability study of catalyst (Reaction conditions: rotation speed of 500 r/min, catalyst loading of 2.5 wt%, alcohol-to-oil mass ratio of 35%, reaction temperature of 60 °C, and reaction time of 2 h).

#### 3.6. Comparison of FAME Production Using the Eggshell-Derived CaO

Table 3 presents a comprehensive overview of scientific experiments utilizing eggshell-derived CaO as a catalyst for biodiesel production. These studies have explored various aspects, such as preparation methods and catalyst preparation conditions, including calcination conditions and hydration processes. In comparison to the studies listed in Table 3, the optimized catalyst employed in this project for the transesterification reaction of glycerol-esterified oil demonstrated notable advantages. Firstly, it achieved a significant reduction in catalyst loading, leading to a more efficient and economical process. Additionally, it exhibited a relatively high yield of FAME within a more suitable temperature range, op-

timizing the reaction conditions for biodiesel production. Furthermore, this optimized catalyst presented remarkable improvements in its cycle life, ensuring enhanced reusability compared to previous studies.

**Table 3.** Summary of the FAME production using the eggshell-derived CaO.

Catalyst			Reaction Conditions				Yield/ Conversion (%)	Reusability (Cycles)	Ref.	
Type	Preparation Method	Calcination Temperature (°C)	Feedstock	Catalyst Amount (wt%)	Alcohol-to- Oil Molar/Mass Ratio	Temperature (°C)				Duration (h)
Loaded CaO (CuFe <sub>2</sub> O <sub>4</sub> )	Precipitation	800	Chicken fat	3.0	15:1 (molar)	70	4.0	94.52 (Y)	-	[49]
Bio-CaO	Calcination	900	Sunflower oil	3.0	9:1 (molar)	60	3.0	97.75 (C)	-	[30]
Supported CaO (SiO <sub>2</sub> )	Impregnation	900	Waste cooking oil	8.0	14:1 (molar)	60	1.5	91.00 (Y)	2	[50]
Bio-CaO	Calcination	800	Palm olein oil	10.0	12:1 (molar)	60	2.0	94.10 (Y)	-	[51]
Bio-CaO	Calcination	900	Palm oil	20.0	9:1 (molar)	60	3.0	94.49 (C)	4	[40]
Hydrated- dehydrated CaO	Calcination- hydration- dehydration- calcination	1st—900 2nd—600	Waste frying oil	5.0	12:1 (molar)	60	1.0	94.52 (C)	6	[33]
Hydrated- dehydrated CaO	Calcination- hydration- dehydration- calcination	1st—900 2nd—800	Waste cooking oil	2.5	12:1 (molar)	60	2.0	94.00 (Y)	-	[52]
Hydrated- dehydrated CaO	Calcination- hydration- dehydration- calcination	1st—875 2nd—725	Glycerol- esterified oil	2.5	35 wt%	60	2.0	94.44 (Y)	8	This Study

#### 4. Conclusions

In this study, an approach that combined glycerol esterification and transesterification reaction to produce biodiesel from high-acid-value oil was proposed. Hydration–dehydration-treated eggshell-derived CaO catalysts were synthesized and applied in the transesterification of glycerol-esterified oil. Using systematic optimization, the optimal catalyst CaOH-60-6h was synthesized under calcination of 875 °C for 3 h, hydration of 60 °C for 6 h, and dehydration of 725 °C. Under the optimal reaction conditions (catalyst loading of 2.5 wt%, alcohol-to-oil mass ratio of 35%, reaction temperature of 60 °C, and reaction duration of 2 h), the yield of FAME of 94.44% was obtained. In addition, the catalyst exhibited excellent reusability, maintaining a yield of FAME at approximately 80% even after eight reaction cycles. Using a comprehensive comparison, the optimized eggshell-derived nano CaO catalyst demonstrates enhanced activity, superior reusability, and milder reaction conditions. Overall, the technique is promising for biodiesel production from high-acid-value oil, with great potential for replacing homogeneous base catalysts for the large-scale production of biodiesel.

**Supplementary Materials:** The following supporting information can be downloaded at: <https://www.mdpi.com/article/10.3390/en16186717/s1>, Figure S1: SEM images of fresh CaO catalyst (without Hydration–dehydration treatment); Figure S2: SEM images of CaO<sub>H-60-6h</sub> catalyst.

**Author Contributions:** Z.W.: Conceptualization, Investigation, Data curation, Writing—original draft. Y.T.: Investigation, Data curation. H.F.: Writing—original draft, Writing—review and editing. W.D.: Investigation, Data curation. Y.C.: Data curation, Visualization. Z.Z.: Formal analysis. X.L.: Funding acquisition, Resources. Y.N.: Funding acquisition, Resources, Project administration, Supervision. All authors have read and agreed to the published version of the manuscript.

**Funding:** This project was supported by the Zhejiang Provincial “Jianbing” “Lingyan” Research and Development Program of China [grant numbers 2022C01191], the National Natural Science Foundation of China (NSFC) [grant numbers 22108249], and the Zhejiang Provincial University Students Science and Technology Innovation Activity Plan (“Xinmiao” Talent Plan) [grant number 2022R403A008].

**Data Availability Statement:** Data will be made available on request.

**Conflicts of Interest:** The authors declare no conflict of interest.

## References

1. Akram, F.; ul Haq, I.; Raja, S.I.; Mir, A.S.; Qureshi, S.S.; Aqeel, A.; Shah, F.I. Current Trends in Biodiesel Production Technologies and Future Progressions: A Possible Displacement of the Petro-Diesel. *J. Clean. Prod.* **2022**, *370*, 133479. [CrossRef]
2. Choudhary, S.; Tripathi, S.; Poluri, K.M. Microalgal-Based Bioenergy: Strategies, Prospects, and Sustainability. *Energy Fuels* **2022**, *36*, 14584–14612. [CrossRef]
3. Liu, Z.; Lian, T.; Li, W.; Cao, C.; Xiong, H.; Li, Y. Mini Review of Current Combustion Research Progress of Biodiesel and Model Compounds for Gas Turbine Application. *Energy Fuels* **2021**, *35*, 13569–13584. [CrossRef]
4. Zulqarnain; Mohd Yusoff, M.H.; Ayoub, M.; Ramzan, N.; Nazir, M.H.; Zahid, I.; Abbas, N.; Elboughdiri, N.; Mirza, C.R.; Butt, T.A. Overview of Feedstocks for Sustainable Biodiesel Production and Implementation of the Biodiesel Program in Pakistan. *ACS Omega* **2021**, *6*, 19099–19114. [CrossRef] [PubMed]
5. Tangy, A.; Pulidindi, I.N.; Dutta, A.; Borenstein, A. Strontium Oxide Nanoparticles for Biodiesel Production: Fundamental Insights and Recent Progress. *Energy Fuels* **2021**, *35*, 187–200. [CrossRef]
6. Maheshwari, P.; Haider, M.B.; Yusuf, M.; Klemeš, J.J.; Bokhari, A.; Beg, M.; Al-Othman, A.; Kumar, R.; Jaiswal, A.K. A Review on Latest Trends in Cleaner Biodiesel Production: Role of Feedstock, Production Methods, and Catalysts. *J. Clean. Prod.* **2022**, *355*, 131588. [CrossRef]
7. Elgharbawy, A.S.; Sadik, W.A.; Sadek, O.M.; Kasaby, M.A. A Review on Biodiesel Feedstocks and Production Technologies. *J. Chil. Chem. Soc.* **2021**, *66*, 5098–5109. [CrossRef]
8. Nie, Y.; Xia, F.; Xie, Q.; Lu, M.; Liang, X.; Su, Y.; Ji, J. Method for Preparing Low-Sulfur Biodiesel 2021. Available online: <https://patents.justia.com/patent/20200095511> (accessed on 2 November 2021).
9. Xie, Q.; Cai, L.; Xia, F.; Liang, X.; Wu, Z.; Liu, Y.; Li, X.; Lu, M.; Nie, Y.; Ji, J. High Vacuum Distillation for Low-Sulfur Biodiesel Production: From Laboratory to Large Scale. *J. Clean. Prod.* **2019**, *223*, 379–385. [CrossRef]
10. Anderson, E.; Addy, M.; Xie, Q.; Ma, H.; Liu, Y.; Cheng, Y.; Onuma, N.; Chen, P.; Ruan, R. Glycerin Esterification of Scum Derived Free Fatty Acids for Biodiesel Production. *Bioresour. Technol.* **2016**, *200*, 153–160. [CrossRef]
11. Demirbas, A. Comparison of Transesterification Methods for Production of Biodiesel from Vegetable Oils and Fats. *Energy Convers. Manag.* **2008**, *49*, 125–130. [CrossRef]
12. Sharma, Y.C.; Singh, B.; Korstad, J. Latest Developments on Application of Heterogeneous Basic Catalysts for an Efficient and Eco Friendly Synthesis of Biodiesel: A Review. *Fuel* **2011**, *90*, 1309–1324. [CrossRef]
13. Leung, D.Y.C.; Wu, X.; Leung, M.K.H. A Review on Biodiesel Production Using Catalyzed Transesterification. *Appl. Energy* **2010**, *87*, 1083–1095. [CrossRef]
14. MacLeod, C.S.; Harvey, A.P.; Lee, A.F.; Wilson, K. Evaluation of the Activity and Stability of Alkali-Doped Metal Oxide Catalysts for Application to an Intensified Method of Biodiesel Production. *Chem. Eng. J.* **2008**, *135*, 63–70. [CrossRef]
15. Boey, P.-L.; Maniam, G.P.; Hamid, S.A. Performance of Calcium Oxide as a Heterogeneous Catalyst in Biodiesel Production: A Review. *Chem. Eng. J.* **2011**, *168*, 15–22. [CrossRef]
16. Gupta, J.; Agarwal, M.; Dalai, A.K. An Overview on the Recent Advancements of Sustainable Heterogeneous Catalysts and Prominent Continuous Reactor for Biodiesel Production. *J. Ind. Eng. Chem.* **2020**, *88*, 58–77. [CrossRef]
17. Patil, P.D.; Deng, S. Transesterification of Camelina Sativa Oil Using Heterogeneous Metal Oxide Catalysts. *Energy Fuels* **2009**, *23*, 4619–4624. [CrossRef]
18. Singh, R.; Kumar, A.; Chandra Sharma, Y. Biodiesel Production from Microalgal Oil Using Barium–Calcium–Zinc Mixed Oxide Base Catalyst: Optimization and Kinetic Studies. *Energy Fuels* **2019**, *33*, 1175–1184. [CrossRef]
19. Aleman-Ramirez, J.L.; Moreira, J.; Torres-Arellano, S.; Longoria, A.; Okoye, P.U.; Sebastian, P.J. Preparation of a Heterogeneous Catalyst from Moringa Leaves as a Sustainable Precursor for Biodiesel Production. *Fuel* **2021**, *284*, 118983. [CrossRef]
20. Faruque, M.O.; Razzak, S.A.; Hossain, M.M. Application of Heterogeneous Catalysts for Biodiesel Production from Microalgal Oil—A Review. *Catalysts* **2020**, *10*, 1025. [CrossRef]
21. Liu, X.; He, H.; Wang, Y.; Zhu, S.; Piao, X. Transesterification of Soybean Oil to Biodiesel Using CaO as a Solid Base Catalyst. *Fuel* **2008**, *87*, 216–221. [CrossRef]
22. Chouhan, A.P.S.; Sarma, A.K. Modern Heterogeneous Catalysts for Biodiesel Production: A Comprehensive Review. *Renew. Sustain. Energy Rev.* **2011**, *15*, 4378–4399. [CrossRef]
23. Li, H.; Wang, Y.; Ma, X.; Wu, Z.; Cui, P.; Lu, W.; Liu, F.; Chu, H.; Wang, Y. A Novel Magnetic CaO-Based Catalyst Synthesis and Characterization: Enhancing the Catalytic Activity and Stability of CaO for Biodiesel Production. *Chem. Eng. J.* **2020**, *391*, 123549. [CrossRef]

24. Mazaheri, H.; Ong, H.C.; Amini, Z.; Masjuki, H.H.; Mofijur, M.; Su, C.H.; Anjum Badruddin, I.; Khan, T.M.Y. An Overview of Biodiesel Production via Calcium Oxide Based Catalysts: Current State and Perspective. *Energies* **2021**, *14*, 3950. [[CrossRef](#)]
25. Boey, P.-L.; Maniam, G.P.; Hamid, S.A. Biodiesel Production via Transesterification of Palm Olein Using Waste Mud Crab (*Scylla Serrata*) Shell as a Heterogeneous Catalyst. *Bioresour. Technol.* **2009**, *100*, 6362–6368. [[CrossRef](#)]
26. Nakatani, N.; Takamori, H.; Takeda, K.; Sakugawa, H. Transesterification of Soybean Oil Using Combusted Oyster Shell Waste as a Catalyst. *Bioresour. Technol.* **2009**, *100*, 1510–1513. [[CrossRef](#)] [[PubMed](#)]
27. Hu, S.; Wang, Y.; Han, H. Utilization of Waste Freshwater Mussel Shell as an Economic Catalyst for Biodiesel Production. *Biomass Bioenergy* **2011**, *35*, 3627–3635. [[CrossRef](#)]
28. Wei, Z.; Xu, C.; Li, B. Application of Waste Eggshell as Low-Cost Solid Catalyst for Biodiesel Production. *Bioresour. Technol.* **2009**, *100*, 2883–2885. [[CrossRef](#)]
29. Buasri, A.; Chaiyut, N.; Loryuenyong, V.; Worawanitchaphong, P.; Trongyong, S. Calcium Oxide Derived from Waste Shells of Mussel, Cockle, and Scallop as the Heterogeneous Catalyst for Biodiesel Production. *Sci. World J.* **2013**, *2013*, 460923. [[CrossRef](#)]
30. Correia, L.M.; Saboya, R.M.A.; de Sousa Campelo, N.; Cecilia, J.A.; Rodríguez-Castellón, E.; Cavalcante, C.L.; Vieira, R.S. Characterization of Calcium Oxide Catalysts from Natural Sources and Their Application in the Transesterification of Sunflower Oil. *Bioresour. Technol.* **2014**, *151*, 207–213. [[CrossRef](#)]
31. Asikin-Mijan, N.; Lee, H.V.; Taufiq-Yap, Y.H. Synthesis and Catalytic Activity of Hydration–Dehydration Treated Clamshell Derived CaO for Biodiesel Production. *Chem. Eng. Res. Des.* **2015**, *102*, 368–377. [[CrossRef](#)]
32. Yoosuk, B.; Udomsap, P.; Puttasawat, B.; Krasae, P. Improving Transesterification Activity of CaO with Hydration Technique. *Bioresour. Technol.* **2010**, *101*, 3784–3786. [[CrossRef](#)]
33. Niju, S.; Meera, K.M.; Begum, S.; Anantharaman, N. Modification of Egg Shell and Its Application in Biodiesel Production. *J. Saudi Chem. Soc.* **2014**, *18*, 702–706. [[CrossRef](#)]
34. Ashine, F.; Kiflie, Z.; Prabhu, S.V.; Tizazu, B.Z.; Varadharajan, V.; Rajasimman, M.; Joo, S.-W.; Vasseghian, Y.; Jayakumar, M. Biodiesel Production from Argemone Mexicana Oil Using Chicken Eggshell Derived CaO Catalyst. *Fuel* **2023**, *332*, 126166. [[CrossRef](#)]
35. Roschat, W.; Phewphong, S.; Thangthong, A.; Moonsin, P.; Yoosuk, B.; Kaewpuang, T.; Promarak, V. Catalytic Performance Enhancement of CaO by Hydration-Dehydration Process for Biodiesel Production at Room Temperature. *Energy Convers. Manag.* **2018**, *165*, 1–7. [[CrossRef](#)]
36. GB/T 5530-2005; Animal and Vegetable Fats and Oils—Determination of Acid Value and Acidity. National Grain Bureau: Beijing, China, 2005.
37. Maquirriain, M.A.; Querini, C.A.; Pisarello, M.L. Glycerine Esterification with Free Fatty Acids: Homogeneous Catalysis. *Chem. Eng. Res. Des.* **2021**, *171*, 86–99. [[CrossRef](#)]
38. Ngamcharussrivichai, C.; Totarat, P.; Bunyakiat, K. Ca and Zn Mixed Oxide as a Heterogeneous Base Catalyst for Transesterification of Palm Kernel Oil. *Appl. Catal. Gen.* **2008**, *341*, 77–85. [[CrossRef](#)]
39. Lee, S.L.; Wong, Y.C.; Tan, Y.P.; Yew, S.Y. Transesterification of Palm Oil to Biodiesel by Using Waste Obtuse Horn Shell-Derived CaO Catalyst. *Energy Convers. Manag.* **2015**, *93*, 282–288. [[CrossRef](#)]
40. Buasri, A.; Chaiyut, N.; Loryuenyong, V.; Wongweang, C.; Khamrsisuk, S. Application of Eggshell Wastes as a Heterogeneous Catalyst for Biodiesel Production. *Sustain. Energy* **2013**, *1*, 7–13. [[CrossRef](#)]
41. Lam, M.K.; Lee, K.T.; Mohamed, A.R. Homogeneous, Heterogeneous and Enzymatic Catalysis for Transesterification of High Free Fatty Acid Oil (Waste Cooking Oil) to Biodiesel: A Review. *Biotechnol. Adv.* **2010**, *28*, 500–518. [[CrossRef](#)]
42. Minaria, M.; Mohadi, R. Preparation and Characterization of Calcium Oxide from Crab Shells (*Portunus Pelagicus*) and Its Application in Biodiesel Synthesis of Waste Cooking Oil, Palm and Coconut Oil. *Sci. Technol. Indones.* **2016**, *1*, 1–7. [[CrossRef](#)]
43. Boro, J.; Konwar, L.J.; Deka, D. Transesterification of Non Edible Feedstock with Lithium Incorporated Egg Shell Derived CaO for Biodiesel Production. *Fuel Process. Technol.* **2014**, *122*, 72–78. [[CrossRef](#)]
44. Yan, S.; Kim, M.; Mohan, S.; Salley, S.O.; Ng, K.Y.S. Effects of Preparative Parameters on the Structure and Performance of Ca–La Metal Oxide Catalysts for Oil Transesterification. *Appl. Catal. Gen.* **2010**, *373*, 104–111. [[CrossRef](#)]
45. Cao, M.; Peng, L.; Xie, Q.; Xing, K.; Lu, M.; Ji, J. Sulfonated Sargassum Horneri Carbon as Solid Acid Catalyst to Produce Biodiesel via Esterification. *Bioresour. Technol.* **2021**, *324*, 124614. [[CrossRef](#)] [[PubMed](#)]
46. Torkzaban, S.; Feyzi, M.; Norouzi, L. A Novel Robust CaO/ZnFe<sub>2</sub>O<sub>4</sub> Hollow Magnetic Microspheres Heterogeneous Catalyst for Synthesis Biodiesel from Waste Frying Sunflower Oil. *Renew. Energy* **2022**, *200*, 996–1007. [[CrossRef](#)]
47. Pandit, P.R.; Fulekar, M.H. Egg Shell Waste as Heterogeneous Nanocatalyst for Biodiesel Production: Optimized by Response Surface Methodology. *J. Environ. Manag.* **2017**, *198*, 319–329. [[CrossRef](#)] [[PubMed](#)]
48. Maniam, G.P.; Hindryawati, N.; Nurfitri, I.; Manaf, I.S.A.; Ramachandran, N.; Rahim, M.H.A. Utilization of Waste Fat from Catfish (*Pangasius*) in Methyl Esters Preparation Using CaO Derived from Waste Marine Barnacle and Bivalve Clam as Solid Catalysts. *J. Taiwan Inst. Chem. Eng.* **2015**, *49*, 58–66. [[CrossRef](#)]
49. Seffati, K.; Honarvar, B.; Esmaeili, H.; Esfandiari, N. Enhanced Biodiesel Production from Chicken Fat Using CaO/CuFe<sub>2</sub>O<sub>4</sub> Nanocatalyst and Its Combination with Diesel to Improve Fuel Properties. *Fuel* **2019**, *235*, 1238–1244. [[CrossRef](#)]
50. Putra, M.D.; Irawan, C.; Udiantoro; Ristianingsih, Y.; Nata, I.F. A Cleaner Process for Biodiesel Production from Waste Cooking Oil Using Waste Materials as a Heterogeneous Catalyst and Its Kinetic Study. *J. Clean. Prod.* **2018**, *195*, 1249–1258. [[CrossRef](#)]

51. Viriya-empikul, N.; Krasae, P.; Nualpaeng, W.; Yoosuk, B.; Faungnawakij, K. Biodiesel Production over Ca-Based Solid Catalysts Derived from Industrial Wastes. *Fuel* **2012**, *92*, 239–244. [[CrossRef](#)]
52. Erchamo, Y.S.; Mamo, T.T.; Workneh, G.A.; Mekonnen, Y.S. Improved Biodiesel Production from Waste Cooking Oil with Mixed Methanol–Ethanol Using Enhanced Eggshell-Derived CaO Nano-Catalyst. *Sci. Rep.* **2021**, *11*, 6708. [[CrossRef](#)]

**Disclaimer/Publisher’s Note:** The statements, opinions and data contained in all publications are solely those of the individual author(s) and contributor(s) and not of MDPI and/or the editor(s). MDPI and/or the editor(s) disclaim responsibility for any injury to people or property resulting from any ideas, methods, instructions or products referred to in the content.